Suppression of toxicity of the mutant huntingtin protein by its interacting compound, desonide

Haikun Song[a,b,1], Cen Wang[a,1], Chenggang Zhu[c,1], Ziying Wang[a], Huiya Yang[a], Peng Wu[a], Xiaotian Cui[a], Juan Botas[d], Yongjun Dang[a], Yu Ding[a,2], Yiyan Fei[c,2], and Boxun Lu[a,2]

[a]Neurology Department at Huashan Hospital, State Key Laboratory of Medical Neurobiology and MOE Frontiers Center for Brain Science, School of Life Sciences, Fudan University, Shanghai 200438, China; [b]Greater Bay Area Institute of Precision Medicine (Guangzhou), Fudan University, Guangzhou, Guangdong 511458, China; [c]Department of Optical Science and Engineering, Shanghai Engineering Research Center of Ultraprecision Optical Manufacturing, Key Laboratory of Micro- and Nanophotonic Structures, Ministry of Education, Fudan University, Shanghai 200438, China; and [d]Molecular and Human Genetics, Baylor College of Medicine, Houston, TX 77030

Edited by Aaron Gitler, Stanford University, Stanford, CA; received August 3, 2021; accepted January 12, 2022 by Editorial Board Member Ulrich Hartl

Identifying inhibitors of pathogenic proteins is the major strategy of targeted drug discoveries. This strategy meets challenges in targeting neurodegenerative disorders such as Huntington's disease (HD), which is mainly caused by the mutant huntingtin protein (mHTT), an "undruggable" pathogenic protein with unknown functions. We hypothesized that some of the chemical binders of mHTT may change its conformation and/or stability to suppress its downstream toxicity, functioning similarly to an "inhibitor" under a broader definition. We identified 21 potential mHTT selective binders through a small-molecule microarray–based screening. We further tested these compounds using secondary phenotypic screens for their effects on mHTT-induced toxicity and revealed four potential mHTT-binding compounds that may rescue HD-relevant phenotypes. Among them, a Food and Drug Administration–approved drug, desonide, was capable of suppressing mHTT toxicity in HD cellular and animal models by destabilizing mHTT through enhancing its polyubiquitination at the K6 site. Our study reveals the therapeutic potential of desonide for HD treatment and provides the proof of principle for a drug discovery pipeline: target-binder screens followed by phenotypic validation and mechanistic studies.

Huntington's disease | movement disorders | neurodegeneration | drug target | desonide

Most neurodegenerative disorders share the common hallmark of the accumulation of misfolded proteins, such as the mutant HTT protein (mHTT) with the expanded polyglutamine (polyQ) stretch, which is the major cause of Huntington's disease (HD) (1). The wild-type HTT protein (wtHTT) may function as a scaffold protein (2), whereas the exact etiology about how mHTT causes HD is unclear, making mHTT an "undruggable" target due to a lack of measurable biochemical readout and "druggable" pockets (binding pockets whose occupancy influences mHTT biochemical functions). As a result, it is believed to be impossible to screen for "inhibitors" of mHTT as potential HD drug candidates.

On the other hand, compounds that bind to mHTT directly may influence its protein structure and, consequently, alter its stability and/or pathogenic functions despite a lack of druggable pockets. In addition, while the exact pathogenic mechanism is unclear, the ultimate functional outcome of mHTT at the cellular level is cytotoxicity, which is measurable in a high-throughput compatible manner. Thus, we may screen for mHTT-binding compounds and then perform secondary phenotypic screens for suppressors of mHTT-induced toxicity. The identified hit compounds may suppress mHTT toxicity by interacting with it directly, providing potential therapeutic leads as well as chemical biology tools to explore HD pathological mechanisms.

In this study, we identified four compounds with such desired properties by these screening strategies. In addition, we performed a counter-screen using the wtHTT to identify the allele-selective binding compounds that interact with mHTT but not wtHTT. Among the hit compounds, desonide, a Food and Drug Administration (FDA)-approved drug for atopic dermatitis (3) and a low-potency topical corticosteroid (4), exhibited robust rescue effects of HD-relevant phenotypes in cells and in vivo in a knockin mouse model, and we further explored the mechanism of action of desonide as well as its therapeutic potential.

Results

Identification of Allele-Selective mHTT-Binding Compounds. To identify compounds that interact with mHTT selectively, we stamped a compound library in duplicates in the format of a small-molecule microarray (SMM) on isocyanate-functionalized glass slides using the nucleophile-isocyanate reaction, which forms covalent bonds between the compounds and the glass slides (Fig. 1*A*) (5). We then flew the recombinant purified GFP-tagged mHTT protein fragment (HTTexon1-Q72-sfGFP; *SI Appendix*, Fig. S1) through the SMM and detected compound–protein interactions by scanning the GFP fluorescent signals (Fig. 1*A*).

Significance

Classical drug discovery identifies inhibitors that block the activities of pathogenic proteins. This typically relies on a measurable biochemical readout and accessible binding sites whose occupancy influences the activity of the target protein. These requirements make many pathogenic proteins "undruggable." Here, we report a strategy to target these undruggable proteins: screening for compounds that directly bind to the undruggable target and rescue disease-relevant phenotypes. These compounds may suppress the target's pathogenic functions via direct binding to it. We applied this strategy to the mutant HTT protein, which is an undruggable protein that causes Huntington's disease (HD). We revealed desonide, an FDAapproved drug, as a possible lead compound for HD drug discovery.

Author contributions: B.L. designed research; H.S., C.W., C.Z., Z.W., H.Y., P.W., and X.C. performed research; J.B. and Y. Dang contributed new reagents/analytic tools; H.S., Y. Ding, Y.F., and B.L. analyzed data; and H.S., Y. Ding, Y.F., and B.L. wrote the paper.

Competing interest: B.L., Y.F., Y. Ding, and Y. Dang are inventors of a relevant patent filed based on this study (Application No. 202110795274.4, to China National Intellectual Property Administration). They are also shareholders of biotech companies whose scopes do not contain this study.

This article is a PNAS Direct Submission. A.G. is a guest editor invited by the Editorial Board.

[1]H.S., C.W., and C.Z. contributed equally to this work.

[2]To whom correspondence may be addressed. Email: yuding@fudan.edu.cn, fyy@fudan.edu.cn, or luboxun@fudan.edu.cn.

This article contains supporting information online at http://www.pnas.org/lookup/suppl/doi:10.1073/pnas.2114303119/-/DCSupplemental.

Published March 1, 2022.

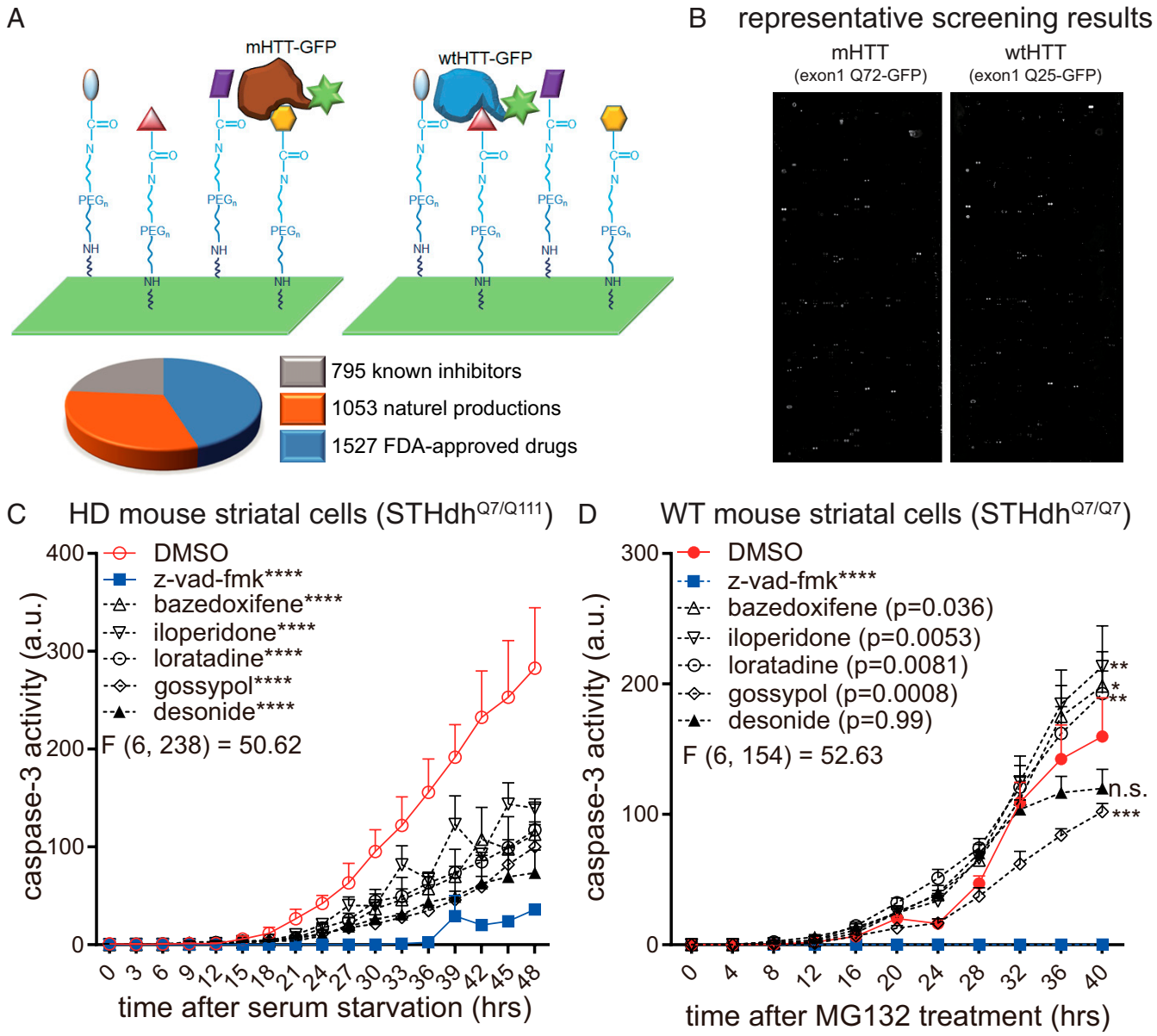

Fig. 1. Identification of potential mHTT-binding compounds that suppressed its cytotoxicity. (*A*) The schematic illustration of the SMM-based primary screening for compounds that selectively interact with mHTT-exon1 (Q72) but not wtHTT-exon1 (Q25) protein fragments. The GFP tag fused with the HTT-exon1 fragments generated signals when interacting with certain compounds stamped at specific spots. Pie chart: categories of compounds stamped onto the SMM chip. (*B*) A representative pair of images (from two repeats using different chips) from the screen revealing the hit compounds of the primary interactor screen. (*C*) The representative data (from ≥7 batches of experiments) of mHTT cytotoxicity in the HD mouse striatal cells (STHdhQ7/Q111) detected by apoptosis at different time points after serum removal, measured using a green fluorescent dye (NucView 488) to detect active caspase-3. Three independently plated wells were tested for each group. (*D*) Similar to *C*, but in WT mouse striatal cells (STHdhQ7/Q7) after treatment of the proteosome inhibitor MG132 (0.5 μM) plus serum removal. Data are mean and SEM analyzed by two-way ANOVA with Dunnett's post hoc tests compared to the DMSO control group. ****$P < 0.0001$.

The wtHTT protein fragment (HTTexon1-Q25-sfGFP; *SI Appendix*, Fig. S1) was used for the counter-screen to identify mHTT-specific binders (Fig. 1 *A* and *B*). We repeated the screen twice and identified 21 reproducible preliminary hits (Fig. 1 and *SI Appendix*, Table S1).

Secondary Phenotypic Screens for Suppressors of mHTT Cytotoxicity. We then investigated whether some of these mHTT-specific binding compounds may ameliorate mHTT-induced cytotoxicity in a cellular HD model, the STHdh$^{Q7/Q111}$ cells (6). These cells exhibit mHTT-dependent apoptosis signals under stress conditions such as serum starvation, and apoptosis signals have been widely used as readouts for mHTT toxicity (7–9). We measured the hit compounds' effects in these cells by the high-content imaging technique. Five out of the 21 hit compounds exhibited reproducible and significant rescue in these cells approximately at the micromolar concentration range (Fig. 1*C* and *SI Appendix*, Fig. S2). Some of these compounds may have nonspecific effects that are mHTT irrelevant. To exclude this possibility, we tested the potential effects on cytotoxicity of these compounds in wild-type (WT) striatal cells (STHdh$^{Q7/Q7}$). We induced mHTT-irrelevant cytotoxicity in these WT cells by treatment with the proteosome inhibitor MG132 (10), which induced apoptosis under serum removal conditions, possibly via accumulation of misfolded proteins and unfolded protein response (11) (Fig. 1*D*). Note that the proteosome inhibitor

treatment was only performed in the WT cells. If the compounds rescued cytotoxicity in the HD cells specifically through mHTT rather than global changes of the proteasome activity or apoptosis pathway, they are not expected to influence the cytotoxicity in the WT cells tested, because there was no mHTT expression in these WT cells and the apoptosis was induced by proteasome inhibition. Among the five hits identified in the screen in HD cells, only gossypol showed a significant rescue effect in the WT cells (Fig. 1*D*), suggesting that a possible nonspecific effect (Fig. 1*D*). In contrast, all the other four compounds showed either no effects (desonide) or marginal exacerbation of the MG132-induced cytotoxicity (bazedoxifene, loratadine, and iloperidone), confirming them as specific suppressors of mHTT-dependent toxicity (Fig. 1*D*). We then further confirmed the phenotypic rescue effects of these four compounds in the HD patient induced pluripotent stem cell (iPSC)-derived neurons by assaying the apoptosis in this model (Fig. 2*A*) and the HD flies expressing the exon 1 fragment or full-length mHTT in the neurons by assaying the climbing behavioral deficits as an index for motor functions (Fig. 2 *B* and *C*). Taken together, desonide, bazedoxifene, loratadine, and iloperidone suppressed mHTT toxicity in various HD models, possibly via interacting with mHTT. We further confirmed the mHTT-specific binding of these compounds and measured their affinity by orthogonal assays including oblique-incidence reflectivity difference (OI-RD) (12) (*SI Appendix*, Fig. S3).

Hit Triaging Based on In Vivo Behavioral Experiments. We then performed pilot studies in a knockin HD mouse model (13) ($Hdh^{Q140/Q140}$at 10 mo of age) to triage the four compounds identified from the mHTT binding and subsequent phenotypic screens. Iloperidone was delivered by intraperitoneal (ip) injections directly for 4 wk, because previous studies suggest that it can penetrate the blood–brain barrier (BBB) (14). Our preliminary data suggest that injection of iloperidone strongly suppressed the baseline open-field and rearing activities, making the mice much less mobile (*SI Appendix*, Fig. S4 *A* and *B*). This is somewhat consistent with the previous observations that

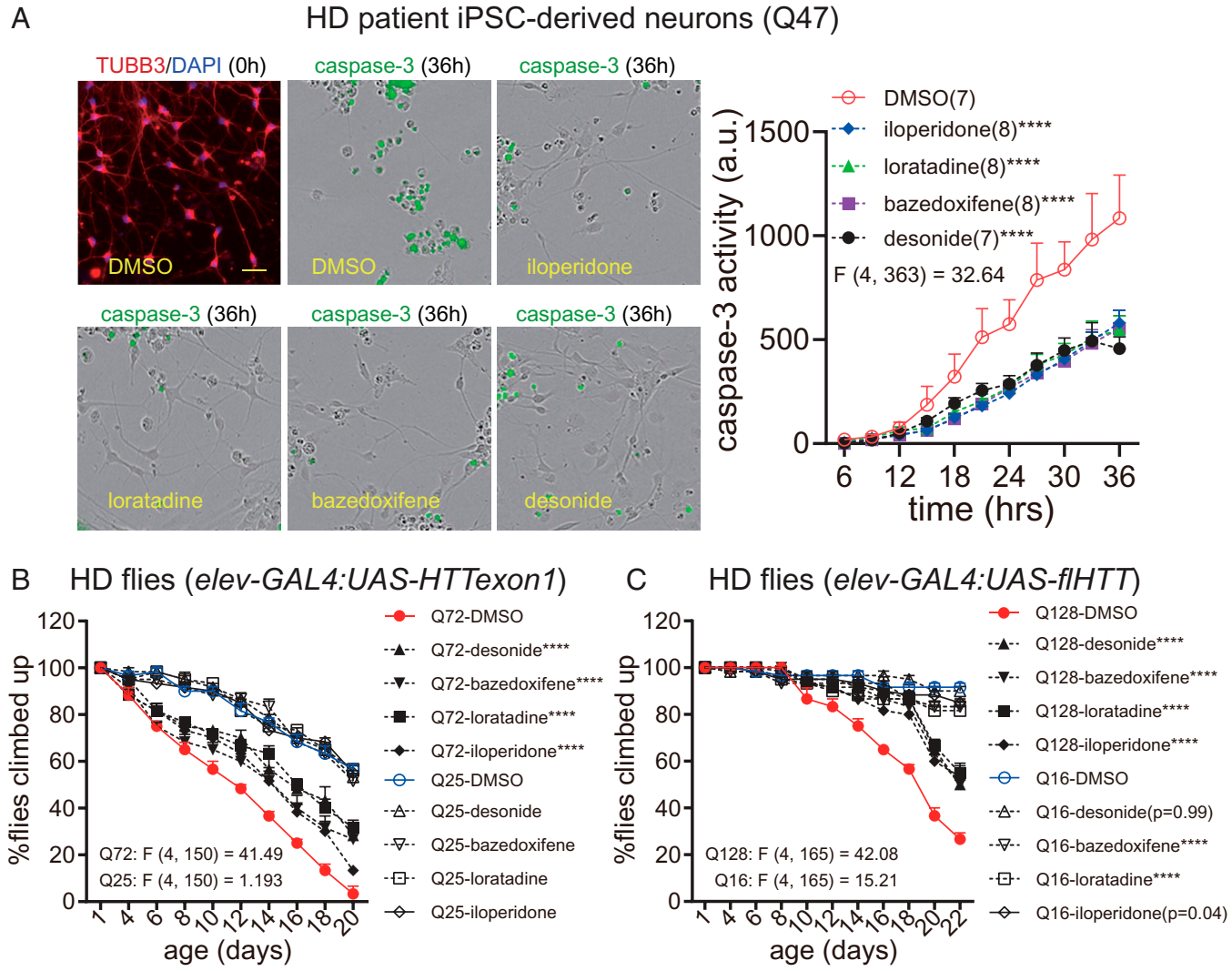

Fig. 2. Phenotypic tests of hit compounds in HD patient iPSC-derived neurons and HD fly models. (*A*) Representative TUBB3 immunofluorescence staining images and Incucyte images with caspase-3 activity quantifications of HD patient iPSC-derived neurons treated with the indicated compounds upon BDNF removal. *n* (the number in parentheses) indicates the number of independently plated wells. (*B* and *C*) Climbing performance of the compound-fed transgenic flies (four vials for each group) as a function of age after eclosion. Data are mean and SEM analyzed by two-way ANOVA with Dunnett's post hoc tests compared to the DMSO control group. ****$P < 0.0001$. Note that all the four tested compounds rescued climbing performance deficits in the HD flies, although bazedoxifene, iloperidone, and loratadine led to a slight decrease of climbing performance in the WT full-length HTT (flHTT-Q16) expressing flies but not the HTTexon1-Q25–expressing flies.

iloperidone suppressed the climbing behavior in mice (14). Thus, the potential effects on HD by iloperidone injection might have been masked by its activity on other targets, and it is hard to pursue with this compound in HD studies.

For the other three compounds, since it is unclear whether they can penetrate the mouse BBB, we delivered them directly to the mouse brain through intracerebroventricular (icv) administrations at a dose estimated based on the cellular experiments (2 mM at 2 μL; ∼4 μM assuming 1 mL total brain volume) for 4 wk with one injection per day. We then assayed the open-field and rearing behaviors (13) as the primary readout for potential HD-relevant phenotypes. Injection of loratadine had no effects, and injection of bazedoxifene had a mild rescue effect (*SI Appendix*, Fig. S4 *A* and *B*). In comparison, desonide led to the most obvious rescue effects in the HD mice by icv injections (*SI Appendix*, Fig. S4 *A* and *B*). In addition, we further ensured its allele-selective binding to mHTT proteins by microscale thermophoresis (MST) (15) (*SI Appendix*, Fig. S4*C*). Desonide interacted with both the exon 1 fragment of mHTT and the full-length mHTT, while it had very low affinity to wtHTT or its exon 1 fragments (*SI Appendix*, Fig. S4*C*). Consistent with previous observations (12), the affinities measured by the OI-RD experiments were higher than those measured by MST, possibly because excessive compounds had been immobilized on the SMM for protein binding in the OI-RD assays. Overall, both assays showed consistent allele-selective desonide–mHTT binding.

icv Injection of Desonide-Rescued HD-Relevant Phenotypes. Thus, we focused on desonide and performed more comprehensive characterization of its effects on different HD-relevant phenotypes, including tests for open-field behaviors, gripping forces, rearing frequencies, beam-walking time, and rotarod performance, which are typical HD-relevant behavioral readouts (16). We also tested desonide's effects in the WT littermates to exclude possible HD-irrelevant artifacts. Consistent with the pilot in vivo studies (*SI Appendix*, Fig. S4 *A* and *B*), desonide-injected HD animals ($Hdh^{Q140/Q140}$, 12 mo old at the start of the 4-wk injection) exhibited significantly improved motor performance in all these behavioral assays (Fig. 3 *A*–*E*), confirming the rescue effects of desonide. Such effects are likely to be specific for HD because the injection in the WT animals showed no effects (Fig. 3 *A*–*E*).

To further confirm desonide's effects at the molecular level in vivo, we assayed the molecular biomarkers of HD, including mHTT aggregates, and the level of DARPP-32, a marker for medium spiny neuron that is lowered in HD (17). Consistent with the behavioral assays, we observed significant lowering of mHTT aggregates and increase of DARPP-32 signals by desonide injections, as well (Fig. 3*F*).

Desonide Lowered mHTT in an Allele-Selective Manner. We then investigated possible mechanisms via which desonide rescued HD-relevant phenotypes. We first investigated whether desonide changed the mHTT protein level, which is a major determinant of its toxicity. Desonide treatment for 48 h significantly reduced the mHTT level in a dose-dependent manner in the $STHdh^{Q7/Q111}$ cells, as detected by Western blots (Fig. 4*A* and *SI Appendix*, Fig. S5*A*), providing the possible explanation of its phenotypic rescue effects in these cells. The wtHTT was not significantly influenced (Fig. 4*A* and *SI Appendix*, Fig. S5*A*), consistent with the observation that desonide only interacts with mHTT but not wtHTT (*SI Appendix*, Figs. S3 and S4*C*).

We further confirmed the allele-specific mHTT-lowering effect of desonide in vivo by ip injection in the heterozygous HD mice ($Hdh^{Q7/Q140}$) (Fig. 4*B*). The mHTT lowering was also confirmed in the HD patient fibroblasts, HD patient iPSC-derived neurons, and HD flies by the homogeneous time resolved fluorescence (HTRF) assay specifically detecting mHTT (Fig. 4 *C*–*E* and *SI Appendix*, Fig. S5*B*). Consistent with the lowering of soluble mHTT levels, desonide treatment also lowered the mHTT aggregates in vivo, as presented earlier (Fig. 3*F*).

Desonide Lowered mHTT via Proteasomal Degradation. Desonide lowered mHTT allele selectively, whereas the mutant and WT *HTT* genes have an identical promoter. Thus, desonide probably lowered mHTT via reducing its stability rather than inhibiting its expression, consistent with the allele-selective binding between mHTT and desonide (*SI Appendix*, Figs. S3 and S4*C*). To further confirm this, we treated the HD cells ($STHdh^{Q7/Q111}$) with the proteasome inhibitor MG132 (18) or with the autophagy inhibitor chloroquine (CQ) (19) and then tested the mHTT-lowering effect of desonide (Fig. 5*A*). The effect was significantly blocked by MG132 but not CQ (Fig. 5*A*), suggesting that desonide lowered mHTT via proteasomal degradation. We further validated this in the HD patient fibroblasts (Fig. 5*B*) and the human embryonic kidney 293T (HEK293T) cells overexpressing the exogenous mHTT exon 1 fragment (Fig. 5*C*, HTTexon1-Q72). Consistent with the proteasomal degradation-mediated mechanism, we observed an obvious inhibition of the mHTT-lowering effects by proteasome inhibitors but not autophagy inhibitors (Fig. 5 *B* and *C*), confirming that desonide enhanced the proteasomal degradation of mHTT. To exclude possible nonspecific effects of the proteasome inhibitors, we blocked the proteasomal activity by knocking down the key proteasome subunit PSMD4 in the cells and observed blunted mHTT-lowering effects by desonide treatment (*SI Appendix*, Fig. S5 *C* and *D*), further validating the idea that desonide enhanced the proteasomal degradation of mHTT. Noticeably, in the HEK293T cells expressing mHTTexon1-Q72, both the soluble and aggregated mHTT levels were significantly reduced by desonide (*SI Appendix*, Fig. S5*D*) as measured by well-established HTRF assays for soluble versus aggregated mHTT (20), confirming that the reduction of soluble mHTT by desonide was not due to decreased solubility.

Desonide–mHTT Interaction Requires K6. To further elucidate the mechanism via which desonide lowered mHTT, we investigated the potential sites in mHTT to which desonide may bind. Previous studies suggest that certain compounds may interact with the expanded polyQ stretch of mHTT and lower several different proteins containing it (12), including the mutant ATXN3, which is the pathogenic protein of spinocerebellar ataxia type 3 (SCA3) (21). This is unlikely to be the case for desonide, which failed to decrease the mutant ATXN3 protein level (Fig. 6*A*). Consistent with this, expanded polyQ stretches fused with the GFP tag failed to interact with desonide (Fig. 6 *B*, *Left*), suggesting that the expanded polyQ stretch alone is insufficient for the binding of desonide. Desonide was able to interact with the mHTT exon 1 fragment (*SI Appendix*, Fig. S3), which mainly consists of the N-terminal 17 amino acids (N17), the expanded polyQ stretch, and the proline-rich domain (PRD). HTTexon1-Q72 lacking PRD (ΔPRD) still interacted with desonide (Fig. 6 *B*, *Right*), suggesting that PRD is not required for the binding. Interestingly, the K6R mutation of N17 abolished binding (Fig. 6 *B*, *Right*). Meanwhile, mutations of the other two lysines (K9 and K15) or the negatively charged amino acid glutamine (E12) in the N17 did not abolish the binding (Fig. 6 *B*, *Right*). To further confirm the K6 dependence of desonide–mHTT interaction, we performed isothermal titration calorimetry (ITC) assays, which also demonstrated allele-selective and K6-dependent interaction between mHTT and desonide (Fig. 6*C*).

Taken together, the K6 site in mHTT is likely required for desonide–mHTT interaction. The binding site may or may not be K6 per se, but the data suggest that the binding site is influenced by K6 and is probably close to the K6 site. Why this interaction is dependent on expanded polyQ is intriguing. There has been a lack of crystal or cryogenic electron

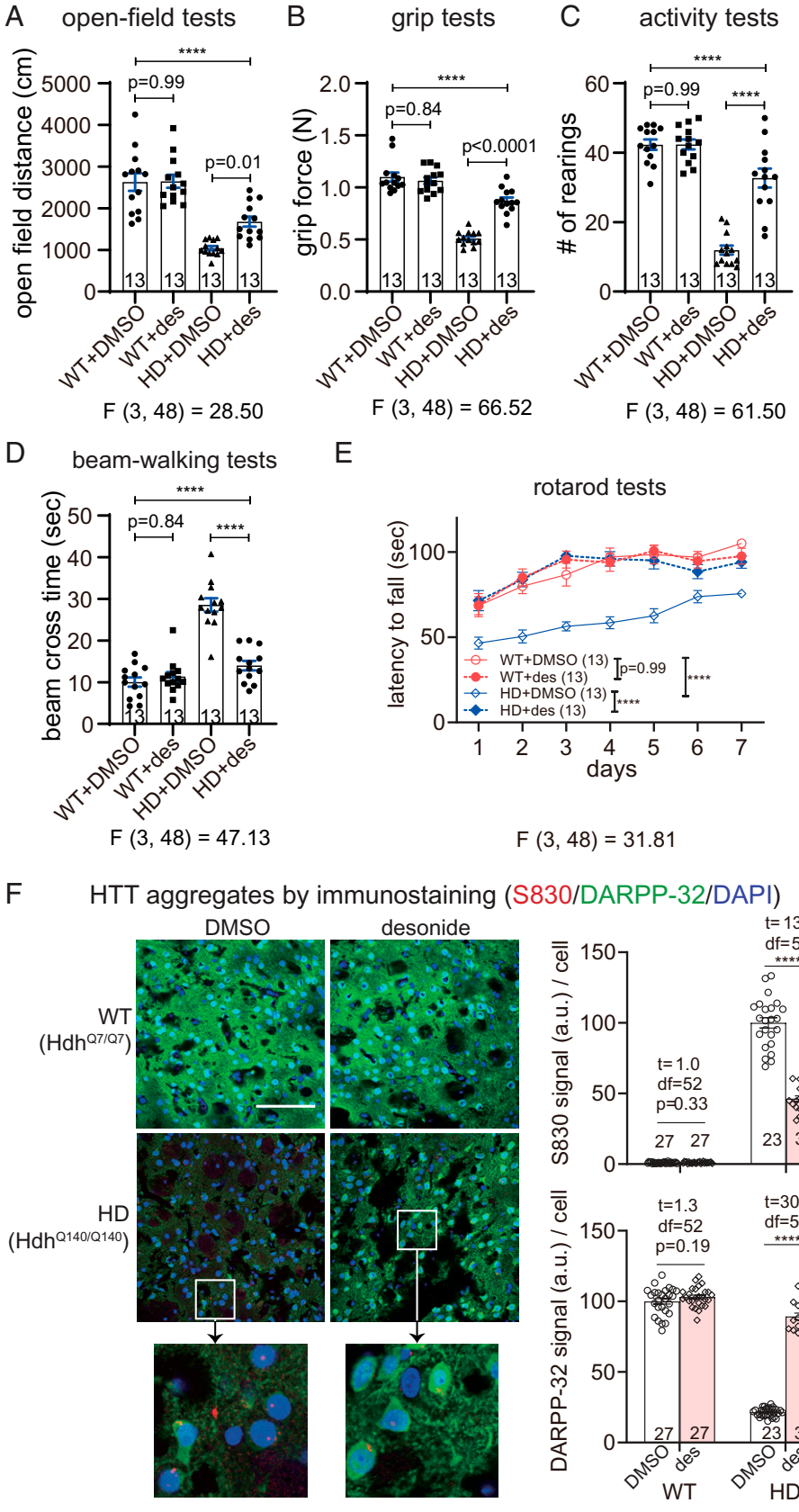

Fig. 3. icv injection of desonide rescued HD-relevant phenotypes in a knockin HD mouse model. (*A–E*) Mouse behavioral tests showing improvement of HD-relevant phenotypes after icv injection of desonide (2 μL at 2 mM) for 4 wk. *n* indicates the number of mice (12 mo old when injection started). (*F*) Representative images and quantifications showing the lowering of mHTT aggregates and increase of DARPP-32 signals by desonide (des) injection as detected by immunostaining with S830 and anti–DARPP-32, respectively. The image analysis was performed by ImageJ in a blinded manner. *n* indicates the number of slices from three mice. (Scale bar, 100 μm.) Data are mean and SEM analyzed by one-way ANOVA (*A–D*) or two-way ANOVA (*E*) with Turkey's post hoc tests or two-tailed unpaired *t* tests (*F*). ****$P < 0.0001$.

microscopy data of the polyQ region of HTT due to its intrinsic unstable conformation (22), making it extremely challenging to address this question by direct structural biology. Meanwhile, the polyQ length regulates the proximity between flanking sequences in HTT, and the N17 and PRD come into close spatial proximity in wtHTT but not mHTT (23). Thus, the PRD

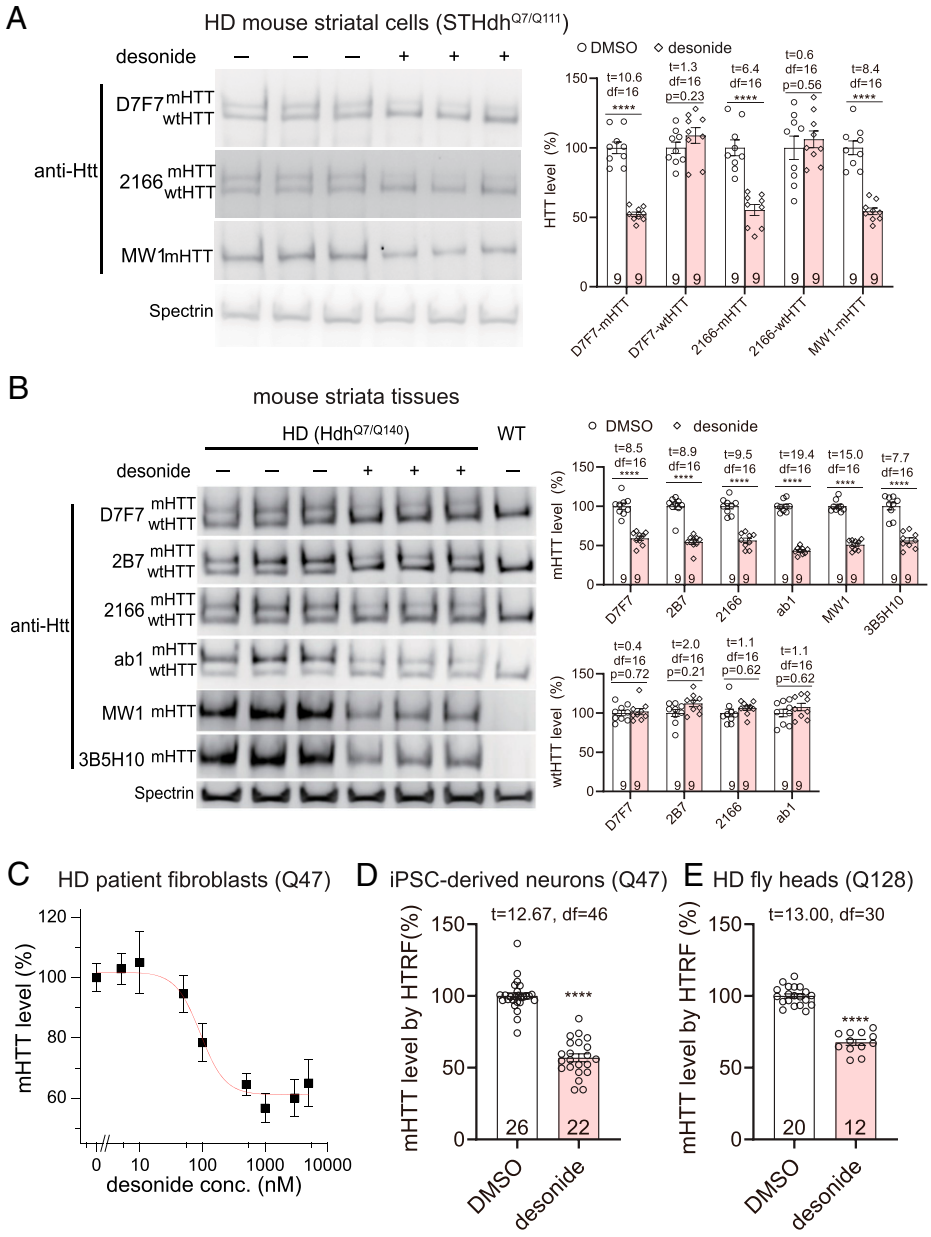

Fig. 4. Desonide lowered mHTT in an allele-selective manner. (*A*) Representative Western blots and quantifications of STHdh cells treated with desonide (3 μM). (*B*) Representative Western blots and quantifications of striata from mice (14 mo old) ip injected with desonide at 5 mg/kg for 4 wk. Nine mice per group were tested. (*C*) The dose–response curve of desonide in HD patient fibroblasts (Q47). mHTT levels were measured by HTRF (the antibody pair: 2B7/MW1; $n \geq 9$). (*D* and *E*) mHTT levels measured by HTRF (2B7/MW1) in HD patient iPSC-derived neurons (*D*, 48 h after 3 μM desonide versus DMSO treatment; *n* indicates the number of independently plated wells) or HD fly heads (*E*, elav-GAL4: UAS-flHTTQ128 fed with the compounds for 6 d after eclosion; *n* indicates the number of vials of flies). Data are mean and SEM analyzed by two-tailed unpaired *t* tests. ****$P < 0.0001$.

following the polyQ region in the wtHTT may fold back to the N17 and shield the site that is crucial for the binding of desonide. In mHTT, the PRD may move away from N17, allowing desonide to bind. This hypothesis is also supported by a structure of HTT exon 1 with 17Q by fusion with an MBP tag, in which PRD forms a kink and folds back, partially covering N17 (24), although the exact region covered in N17 is influenced by the environment of the protein.

Desonide Enhanced the K6 Polyubiquitination of mHTT. We then investigated the mechanism of the lowering of mHTT by desonide. Consistent with the enhanced proteasomal degradation of mHTT, desonide treatment led to an obvious increase of polyubiquitination (poly-ub) of mHTT in HEK293T cells (Fig. 7 *A*, *Left*). The cells were treated with the proteasome inhibitor epoxomicin so that the poly-ub proteins remain in the cells for detection. The increased poly-ub was only observed in the mHTT, but not wtHTT, exon 1 fragment (Fig. 7 *A*, *Left*), consistent with the allele-selective binding of desonide. The K6R mutation completely blocked the enhanced poly-ub of HTTexon1-Q72 by desonide treatment (Fig. 7 *A*, *Middle*), whereas K9R and K15R had no effects (Fig. 7 *A*, *Right*).

Consistent with this, the HTTexon1-Q72 K6R mutant protein was not lowered by desonide treatment, which could lower the levels of mHTTexon1-Q72 or its K9R, K15R, E12A, or S13,16A mutants (Fig. 7*B* and *SI Appendix*, Fig. S6). The K6 dependence of desonide's effects was also confirmed at the functional level. We assayed mHTT cytotoxicity by measuring the apoptosis signal (caspase-3 activity) in HEK293T cells expressing HTTexon1-Q72 versus Q25 fragments under serum-starved conditions (Fig. 7*C*). Desonide suppressed the cytotoxicity induced by expression of the HTTexon1-Q72 or its point mutated forms including K9R, K15R, E12A, and S13,16A in the HEK293T cells (Fig. 7*D* and *SI Appendix*, Fig. S6) but not the cytotoxicity induced by HTTexon1-Q72 K6R expression (Fig. 7*D*). Similar observations were made in WT mouse striatal cells STHdh transfected with HTT exon 1 fragments as well (Fig. 7 *E* and *F*). While the K6R mutation abolished the effects of desonide on mHTT levels, poly-ub, and cytotoxicity (Fig. 7 *A*–*F*), the data alone is insufficient to demonstrate that the

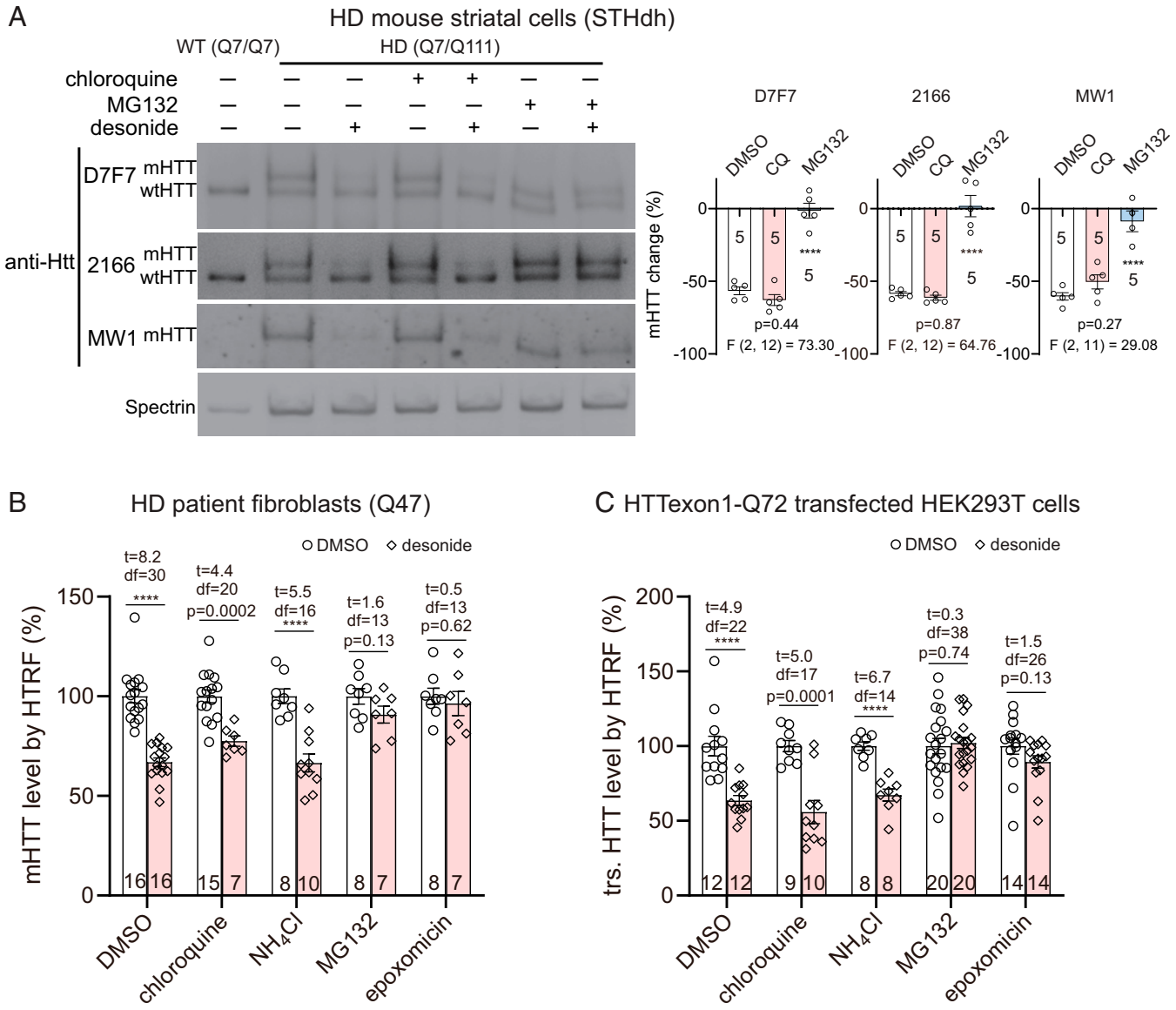

Fig. 5. Desonide lowered mHTT via the proteasome. (*A*) Representative Western blots and quantifications of the mHTT-lowering effects by the desonide treatment in STHdhQ7/Q111 cells with or without indicated inhibitors for proteasome or autophagy. (*B*) HTRF (2B7/MW1) measurements of endogenous mHTT levels in HD patient fibroblasts (Q47) with the indicated compounds. (*C*) HTRF (2B7/MW1) measurements of HTTexon1-Q72 protein levels in transfected HEK293T cells treated with the indicated compounds. In all cells tested, desonide's effects on mHTT lowering were blocked by the proteasome inhibitors, such as MG132 (2 μM) or epoxomicin (100 nM), but not autophagy inhibitors such as NH4Cl (10 mM) or CQ (25 μM). All signals were normalized to the average signals from the DMSO control group. Data are mean and SEM analyzed by two-tailed unpaired *t* tests. ****$P < 0.0001$. *n* indicates the number of independently plated wells.

poly-ub site was K6, because the K6R mutation also abolished desonide–mHTT interaction (Fig. 6). Meanwhile, there are only three lysines in the HTTexon1 protein fragment, K6, K9, and K15. Both K9R and K15R mutations failed to ameliorate desonide's effects on poly-ub of HTTexon1 Q72 (Fig. 7*A* and *SI Appendix*, Fig. S6*B*). Thus, K9 and K15 are unlikely to be the poly-ub site mediating desonide's effects, and K6 is the only possible site. Taken together, desonide enhanced poly-ub of mHTT most likely at the K6 site and increased its proteasomal degradation, leading to reduced mHTT cytotoxicity.

Desonide Did Not Influence mHTT via the Glucocorticoid Receptor. Desonide is known to activate the glucocorticoid receptor (GR), although the potency is low (4). To exclude the potential involvement of GRs, we tested the other GR agonists in the HD cells. These agonists did not interact with mHTT and did not lower its level (*SI Appendix*, Fig. S7*A*). To further exclude the involvement of GR, we knocked down GR and then treated these cells with desonide versus the dimethylsulfoxide (DMSO) control. Desonide was still able to lower mHTT when GR was knocked down (*SI Appendix*, Fig. S7*B*), further confirming that desonide lowered mHTT via GR-independent mechanisms.

Peripheral Delivery of Desonide Rescued HD-Relevant Phenotypes at Different Ages. Desonide is an FDA-approved drug for atopic dermatitis with an established safety profile for external applications (3), but repurposing it to treat HD may need additional clinical studies due to the likely requirement of changing the delivery methods. The icv administration of desonide was effective (Fig. 3), but the delivery approach was infeasible for HD

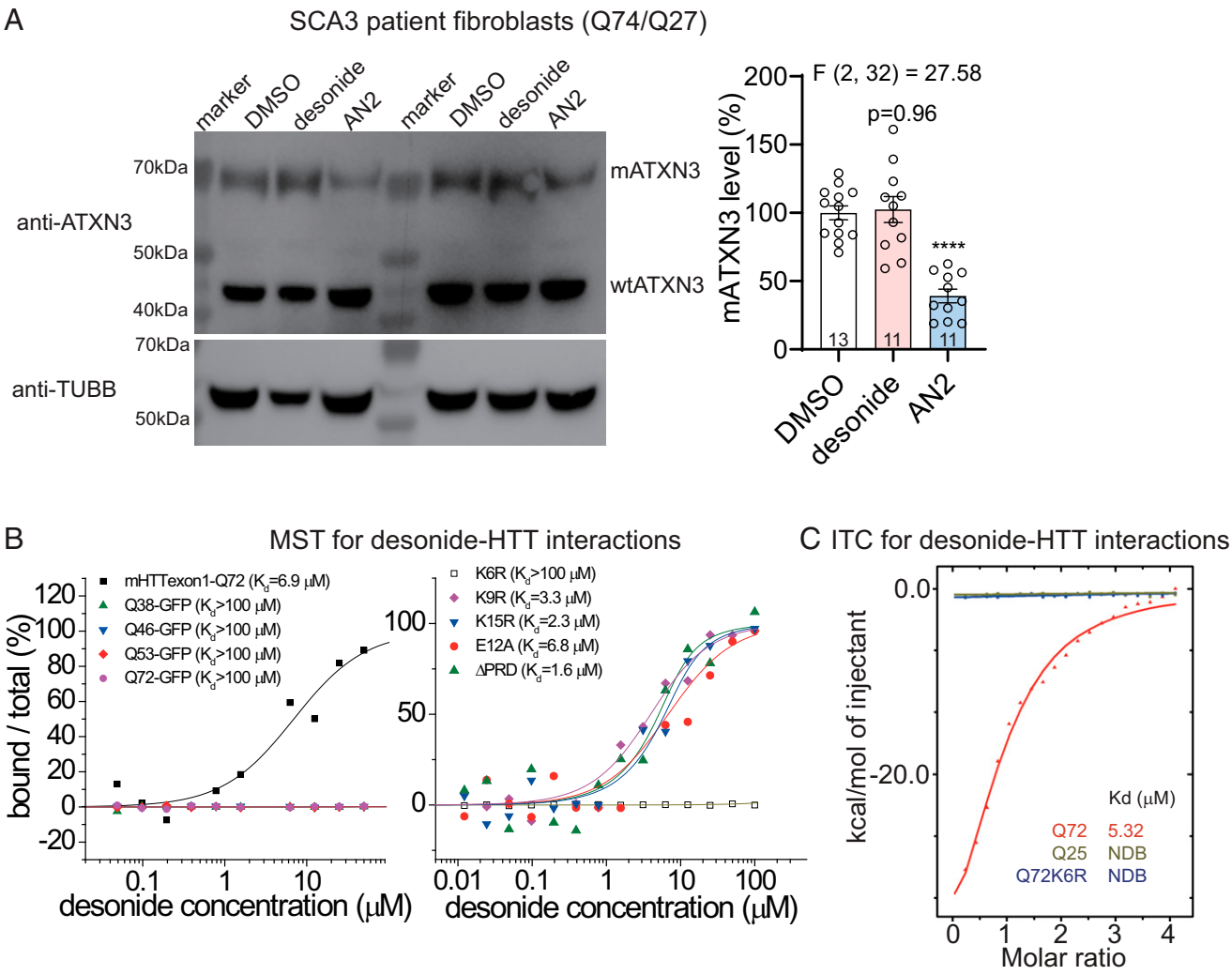

Fig. 6. The desonide–mHTT interaction was dependent on K6 and expanded polyQ. (*A*) Representative Western blots and quantifications of SCA3 patient fibroblasts treated with desonide (3 μM) or the positive control 5,7-dihydroxy-4-phenylcoumarin (AN2, 100 nM) (12). Desonide failed to reduce the level of mutant ATXN3, suggesting that the effect required regions of the HTT protein other than the expanded polyQ stretch. Data are mean and SEM analyzed by one-way ANOVA with Dunnett's post hoc tests. ****$P < 0.0001$. *n* indicates number of independently plated wells. (*B*) Measurements of desonide's binding affinity with the indicated polyQ or HTTexon1 fragments by MST. The long polyQ strength fused with GFP failed to interact with desonide (*Left*). In addition, the K6R mutation abolished the binding between desonide and the HTTexon1-Q72 protein, whereas deletion of the ΔPRD or mutation of the other amino acids did not influence the interaction (*Right*). (*C*) Representative ITC analyses (from two batches of experiments) of desonide–HTT interactions. Curve fitting was performed by using the one-site model (for Q72: $n = 0.910$; $\Delta H = -5.266 \times 104$ cal/mol; $\Delta S = -152$ cal/mol/deg). NDB: no detectable binding.

patients, and validating the possibility of peripheral delivery is critical. To test this possibility, we performed a preliminary pharmacokinetic study and discovered that the brain concentration of desonide may reach ∼2 to 3 μM by 5 mg/kg ip injection (*SI Appendix*, Fig. S8). In addition, the ip injection significantly lowered mHTT in an allele-selective manner (Fig. 4*B*). Thus, we test the potential effects on HD-relevant phenotypes of $Hdh^{Q7/Q140}$ mice at different ages by ip injection of desonide (Fig. 8). At the ages of 10, 12, and 15 mo, all the behavioral deficits tested in the HD mice were rescued by 4 wk of injection by desonide (Fig. 8 *A*–*E*). The WT mice were not influenced, suggesting that the desonide's effect was specific (Fig. 8 *A*–*E*). In addition, the mHTT aggregates were lowered (Fig. 8*F*) and the levels of HD molecular biomarkers, including DARPP-32 and neurofilament light chain (NFL), were partially restored (*SI Appendix*, Fig. S9), confirming the therapeutic potential of desonide for HD treatment. Note that we tested NFL in the brain slices instead of the cerebrospinal fluid (CSF); thus, reduced NFL is an indicator of neurotoxicity in vivo.

Discussion

Our study revealed desonide as a direct binder and an allele-selective modifier of mHTT (Figs. 4 and 6*C* and *SI Appendix*, Figs. S3 and S4*C*). We further demonstrated its potential for HD treatment (Fig. 8), although more thorough studies with additional dosages and models are needed for desonide before entering the clinical phase. As an FDA-approved drug for atopic dermatitis, the safety profile as well as the pharmacokinetic and pharmacodynamic properties have been studied, facilitating its repurposing for HD, although these may need to be retested because the formulation and delivery methods need to be modified for HD treatment.

The suppression of mHTT-induced toxicity by desonide is probably mediated by the desonide–mHTT interaction. First,

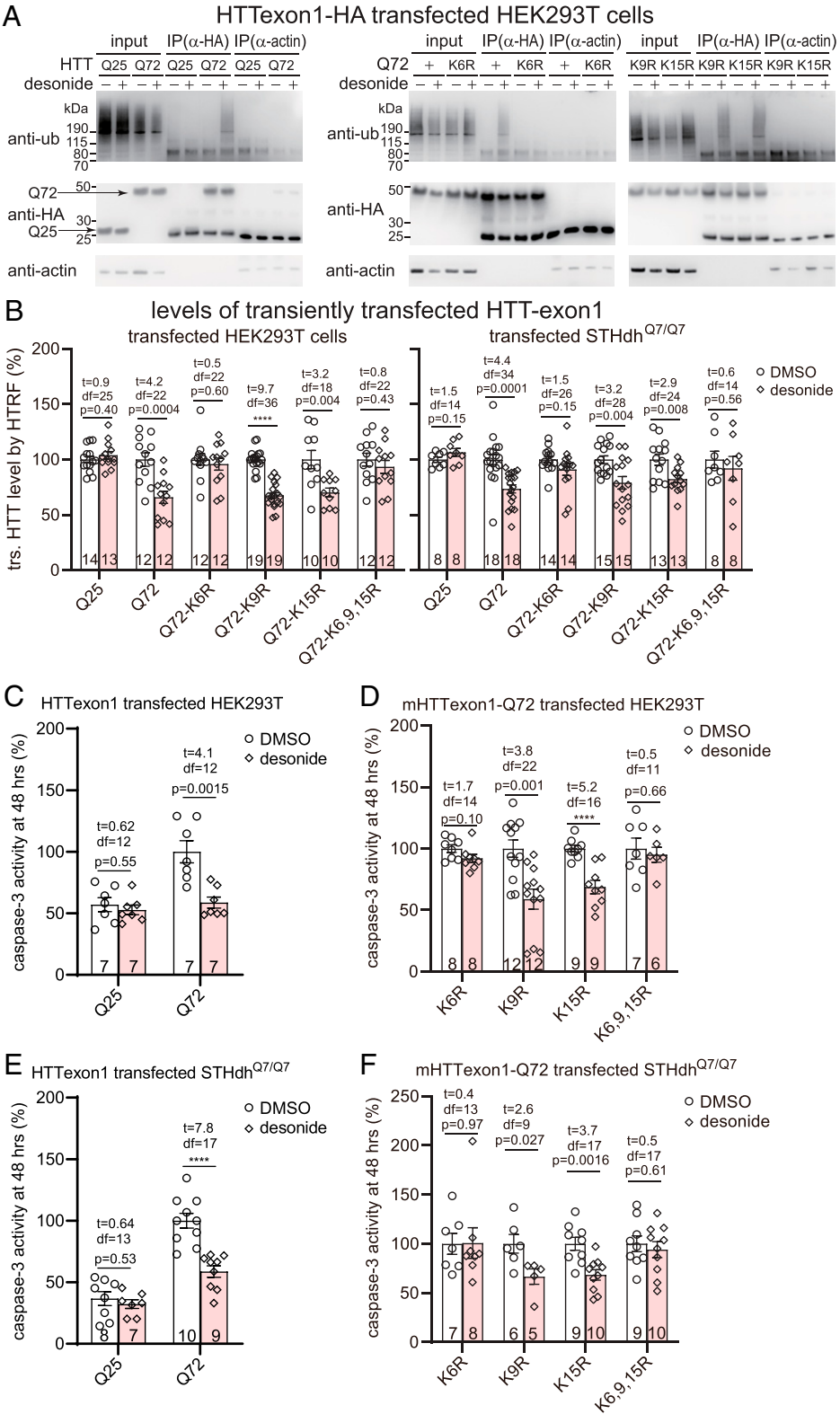

Fig. 7. Desonide lowered mHTT via enhancing its K6 poly-ub. (*A*) Representative immunoprecipitation (IP)-Western results (from five batches) in transfected HEK293T cells showing that desonide enhanced the mHTTexon1-Q72 but not mHTTexon1-Q25 poly-ub, which is abolished by the K6R, but not the K9R or K15R, mutation. Note that the Q25 protein is just slightly above the IgG light chain. (*B*) HTT levels measured by HTRF (2B7/MW1) in transfected HEK293T or STHdhQ7/Q7 cells. All the data were normalized to the DMSO-treated group to exhibit the effects of desonide treatment. (*C*) Caspase-3 activity measurement of HEK293T cells transfected with the indicated HTTexon1 fragments for 24 h and then treated with desonide or DMSO in serum-free medium. Data were normalized to the Q72-transfected and DMSO-treated groups, which showed higher caspase-3 activity than the Q25-transfected groups, illustrating an mHTT-dependent and desonide-sensitive cytotoxicity signal. (*D*) Similar to *C* but transfected with Q72 fragments with indicated point mutations. All the data were normalized to the DMSO-treated group to exhibit the effects of desonide treatment. (*E* and *F*) Similar to *C* and *D* but in STHdhQ7/Q7 cells. Data are mean and SEM analyzed by two-tailed unpaired *t* tests. ****$P < 0.0001$. *n* indicates the number of independently plated wells.

the interaction was allele selective (Fig. 6*C* and *SI Appendix*, Figs. S3 and S4*C*), consistent with the allele selectivity of the mHTT-lowering effects of desonide (Fig. 4). Second, the HTTexon1-Q72 K6R mutant that did not interact with desonide was also resistant to the desonide-mediated mHTT-lowering and cytotoxicity-suppression effects (Figs. 6 and 7), although this could also be explained by the possible requirement of K6 poly-ub for suppression of mHTT-induced toxicity. Finally, the known target of desonide, GR, is unlikely to mediate the rescue and the mHTT-lowering effects (*SI Appendix*, Fig. S7). Meanwhile, we cannot completely exclude the possibility that desonide may suppress mHTT toxicity via other mechanisms.

The observation that K6R mutation abolished the binding of desonide suggests that K6 is very close to the binding site, and

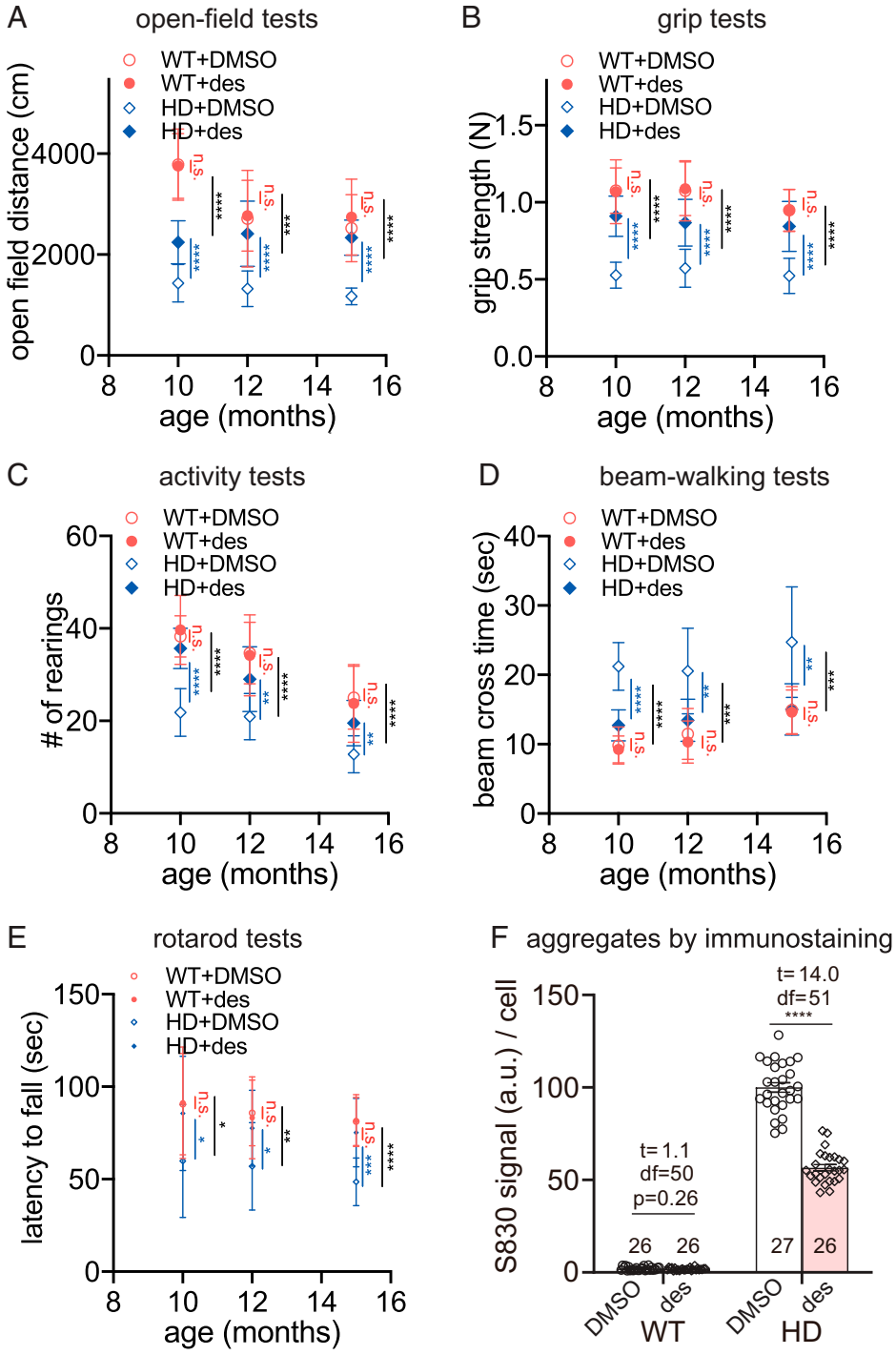

Fig. 8. Peripheral delivery of desonide rescued HD-relevant phenotypes. Mice of indicated genotypes at the age of 9 mo (n = 15), 11 mo (n = 13), or 14 mo (n = 13) were ip injected with desonide at 5 mg/kg for 4 wk with one injection per day. (*A*–*E*) the indicated behavioral analysis demonstrating the rescue effects of desonide in HD mice (HdhQ7/Q140). (*F*) Quantifications of HTT aggregates by immunostaining of striatal brain slices showing the lowering of mHTT aggregates by desonide injection in the striatal tissue from the HD mice at 15 mo of age (injected at 14 mo of age for 4 wk). The aggregates were quantified blindly by ImageJ. n indicates the number of striatal slices from three mice in each group. Data are mean and SD (SEM was too small to be shown) analyzed by unpaired two-tailed t tests. ****$P < 0.0001$.

the K6R mutation may change the conformation of the binding pocket of desonide. Desonide may interact with mHTT and influence the conformation around the K6 site so that it becomes more accessible to its E3 ligase(s), which enhances the K6 poly-ub. Alternatively, desonide's binding may inhibit the recognition of K6 by a deubiquitinase (DUB), leading to reduced deubiquitination. Finally, we cannot exclude the contribution from other modifications such as K6 acetylation (25), which may also influence poly-ub indirectly.

Undruggable targets like mHTT inspired scientists to establish many powerful strategies to overcome the hurdles of identifying inhibitors for such targets: gene therapies, degraders, genetic or chemical modifiers of the target levels, enhancement of autophagy, etc. (1, 26–29). Meanwhile, if we expand the definition of inhibitors to compounds that directly interact with the target and inhibit its ultimate pathogenic functional impacts, such as cell death or disease-relevant phenotypes, we may still be able to identify "inhibitors" for these undruggable targets under this broader definition. Our study demonstrates a potential screening approach to identify such inhibitors: we may first screen for direct binding compounds of the target and then perform phenotypic screens to reveal the suppressors of the downstream cellular phenotypes with proper counter screens to exclude nonspecific artifacts. The hits could then be further triaged by additional phenotypic and mechanistic studies, and the identified compounds may suppress the disease-relevant

phenotypes via direct engagement of the target. The identified mHTT inhibitors by this approach may provide lead compounds for HD treatment or tool compounds for mechanistic studies. This screening strategy could potentially be applied to other undruggable targets as well.

Materials and Methods

Complementary DNA Plasmids and Recombinant Protein Purifications. For details, see *SI Appendix* due to space limits.

SMM Screening. To screen for compounds binding to HTTexon1-Q72 but not to HTTexon1-Q25, SMMs with 3,375 compounds were immersed into the blocking solution (0.5 mg/mL bovine serum albumin [BSA] in phosphate-buffered saline [PBS]) at room temperature for 30 min to block the unused sites and then rinsed three times with PBS. The indicated recombinant purified proteins were applied to the SMM and incubated at room temperature for 120 min. After rinsing with PBS for 20 min, the microarray was ready for image scanning using a commercial fluorescence scanner with excitation wavelength at 488 nm. The bright spots in the fluorescence images indicate compounds that bind to the probing protein.

Compound–Protein Interaction Measurements by OI-RD. To measure the binding kinetics of target proteins with compounds, we prepared SMMs consisting of desonide, iloperidone, loratadine, and bazedoxifene. Six identical microarrays were printed on one glass slide, and each compound was printed in triplicate in a single microarray. The printed small SMMs were assembled into a fluidic cartridge with each microarray housed in a separate chamber. Before the binding reaction, the slide was washed in situ with a flow of 1× PBS to remove excess unbound samples, followed by blocking with 7,600 nM BSA in 1× PBS for 30 min. For binding kinetics measurement, 1× PBS was first flowed through a reaction chamber for 5 min. The 1× PBS was then replaced with the probe solution for 35 min for the association phase of the reaction. The probe solution was then replaced with 1× PBS to allow dissociation of the probe for 30 min. By repeating the binding reactions of the target protein at three different concentrations on separate fresh microarrays, binding curves of compounds with the target protein at three concentrations were recorded with a scanning OI-RD microscope. Reaction kinetic rate constants were extracted by fitting the binding curves globally using the one-to-one Langmuir reaction mode.

Mouse Models. The generation and characterization of the Hdh^{140Q} knockin mice have been previously described (13). The original mice utilized to start to colony were kind gifts from Marian Difiglia's group, Massachusetts General Hospital, Boston, MA. Mice were group housed (up to five adult mice per cage) in individually vented cages with a 12-h light/dark cycle. The mouse experiments were carried out following the general guidelines published by the Association for Assessment and Accreditation of Laboratory Animal Care. The Animal Care and Use Committee of the School of Medicine at Fudan University approved the protocol used in the animal experiments (Approval Nos. 20140904 and 20170223-005). For protein extraction from the mouse brain, the brains were collected and the striata were acutely dissected.

Mouse Behavioral Experiments. For details, see *SI Appendix* due to space limits.

Cell-Culture and Cell-Line Generation. For details, see *SI Appendix* due to space limits.

HD *Drosophila* Models and Behavioral Experiments. The nervous system driver line elav-GAL4 (c155) and the HTT-expressing lines UAS-flHTT-Q16 and UAS-flHTT-Q128 (expressing human full-length HTT with 16Q and 128Q, respectively, when crossed to the GAL4 line) were obtained from the Bloomington *Drosophila* Stock Center at University of Indiana (http://flystocks.bio.indiana.edu/) and maintained in a 25 °C incubator. Crosses were set up between virgin female flies carrying the elav-GAL4 driver and the UAS-flHTT-Q16 or UASflHTT-Q128 male flies to generate the desired genotypes. The UAS-HTT-exon1-Q72 line was generated by injecting the pUAST-HTT-exon1-Q72 vector into w1118 *Drosophila* embryos, and the UAS-HTT-exon1-Q72 line was integrated into chromosome 2. This line expresses an N-terminal human Htt exon 1 fragment with 72Q when crossed with the GAL4 line, and the expression was validated by HTRF.

For behavioral experiments, we placed 15 age-matched virgin female flies in an empty vial and taped them down. The percentage of flies that climbed past a 7-cm-high line after 15 s was recorded. The mean of four observations is plotted for each vial on each day, and data from multiple vials containing different batches of flies were plotted and analyzed by two-way ANOVA tests. The flies were randomly placed into each tube. The person who performed the experiments was blinded to the drugs fed until data analysis.

Compound Treatment in Cells and Animals. For details, see *SI Appendix* due to space limits.

Protein Extraction and Protein Detection by Western Blots and HTRF. The cell pellets were collected and lysed on ice for 30 min in 1× PBS + 1% Triton X-100 + 1× Complete protease inhibitor (Roche, cat. No. 4693159001), sonicated on ice, and spun at >20,000 × *g* at 4 °C for 10 min. The supernatants were then loaded and transferred onto nitrocellulose membranes for Western blots. For mouse brain tissues, the mouse striata were dissected on ice and grinded by a tissue grinder for 5 min at 60 Hz and lysed on ice for 60 min in brain lysis buffer (50 mM Tris, 250 mM NaCl, 5 mM ethylene diamine tetraacetic acid, and 1% Triton X-100, pH 7.4) + 1× Complete protease inhibitor (Roche, cat. No. 4693159001). The samples were then spun at >20,000 × *g* at 4 °C for 15 min. For Western blots, the samples were loaded onto the sodium dodecyl sulphate–polyacrylamide gel electrophoresis gel (3 to 8 or 4 to 12%, depending on the molecular weight of the protein of interest). The proteins on the gel were then transferred to the nitrocellulose membranes for blocking and antibody detection. The signal was detected with ECL (Thermo Fisher Scientific, cat. No. 34577) after 1 h incubation of the membrane with secondary antibody 1:5,000. The HTT antibodies 2B7 (30), MW1 (31), and 4C9 (32) have been described previously. The antibody S830 for immunostaining of HTT aggregates is a kind gift from Gillian Bates, King's College London, London, UK. Commercially purchased antibodies include HTT antibody 2166 (Millipore, cat. No. MAB2166), 3B5H10 (Sigma, No. P1874), anti–β-tubulin (Abcam, cat. No. ab6046), anti-TUBB3 (Covance, cat. No. MMS-435P), anti–DARPP-32 (Abcam, cat. No. ab40801), anti-ATXN3 (Millipore, cat. No. MAB5360), anti-spectrin (Millipore, cat. No. MAB1622), anti-GR (Abmart, cat. No. T56612), anti-HA (Abmart, cat. No. M20003), anti-ubiquitin (ProteinTech, cat. No. 10201-2-AP), and anti-Actin (Abmart, cat. No. M20011). All the antibodies used in this study have been validated either in this study and/or previous literature (cited or indexed in Antibodypedia). The cell or tissue lysates were diluted with the original lysis buffer PBS + 1% (vol/vol) Triton X-100 + 1× complete protease inhibitor (Roche), used for lysing the samples, and then detected with indicated antibody pairs diluted in the HTRF assay buffer (50 mM NaH_2PO_4, 400 mM NaF, 0.1% BSA, 0.05% [vol/vol] Tween-20, and 1% [vol/vol] Triton X-100, pH 7.4). The donor antibody concentration was 0.023 ng/μL, and the acceptor antibody concentration was 1.4 ng/μL, both in HTRF assay buffer. The signals were normalized to the total protein concentrations to ensure equal loadings. Different protein concentrations were pretested to ensure that the signals were in the linear range.

For all the samples, the protein concentrations (by BCA, Beyotime, cat. No. P0009) were measured to correct the loadings. Different protein concentrations or cell numbers per well were tested to ensure that the signals were in the linear range. Background corrections were performed by subtracting the background signals from blank samples.

Immunoprecipitation. HEK293T cells were transiently transfected with HTTexon1Q72-HA constructs and other indicated plasmids or controls (Fig. 7*A*) in 6-well plates for 24 h, and the cells were treated with 100 nM epoxomicin for another 24 h. The cell pellets were collected and lysed on ice for 30 min in 1× PBS + 1% Triton X-100 + 1× complete protease inhibitor (Roche, cat. No. 4693159001), sonicated on ice, and spun at >20,000 × *g* at 4 °C for 10 min. The SureBeads Magnetic Bead Immunoprecipitation System (Bio-Rad, No. 161-4023) was used to pull down the hemagglutinin (HA)-tagged HTT-exon 1. The proteins were then eluted with the gel-loading buffer (lithium dodecyl sulfate buffer with NuPAGE reducing reagent [Thermo Fisher Scientific, cat. No. NP0004]). The inputs and eluates were then loaded on a 4 to 12% Bis-Tris NuPAGE gel for Western blot analysis, in which we used a secondary antibody with only the light chain immunoglobulin G (IgG) to avoid heavy chain interference (Abmart, No. M21004).

Immunofluorescence. For details, see *SI Appendix* due to space limits.

Compound–Protein Interaction Measurements by MST. For details, see *SI Appendix* due to space limits.

ITC Assays to Measure Binding Affinities In Vitro. We used the Malvern's PEAQ-ITC for the ITC experiments. For each experiment, 280 μL 10 μM purified proteins in ITC buffer (20 mM Hepes, pH 7.0, 100 mM NaCl, and 0.2% DMSO) was injected into the cell, and compounds (20 μM) in the same buffer were injected 20 times (0.4 μL for the first drop, 2 μL for drops 2 through 20) with a 180-s interval between injections at a constant temperature of 25 °C, and the

NEUROSCIENCE

heat released by the binding was recorded in real time. Repeated titrations were carried out. The heat released or absorbed by molecular binding was directly proportional to the number of bound molecules. When the system was saturated, only the heat of dilution could be observed. Data were analyzed with Origin software using the One Sites fitting model, and data from the last five injections were used as the baseline.

Immunofluorescence and Caspase-3 Imaging. For details, see *SI Appendix* due to space limits.

siRNA Transfection. The small interference RNAs were reversely transfected into the STHdh cells with lipofectamine 2000 (Life Technologies, No. 11668). All transfections were performed according to the manufacturer's protocol. Cells were collected 3 d after siRNA transfection for Western blot, HTRF, or immunofluorescence. The siRNA target sequences and/or order information are as follows: Non-targeting negative control (Neg) siRNA: nontargeting siRNA (Generalbiol; cat. No. RX028810); GR siRNA: targeting GGUAAUUAAGCAAGAGAAATT;PSMD4-Homo:CCUUAUCACACUGGCUAAUTT; PSMD4-mouse: AGAAAGAGGAAGAGAAGAATT.

Compound Concentration Measurements in Brain Tissues and Plasma from Injected Mice. For details, see *SI Appendix* due to space limits.

Statistics. To ensure reaching a statistical power >0.8, power analyses were performed for each assay based on estimated values by NCSS-PASS (https://www.ncss.com/) before experiments, and we determined $n > 5$ for behavioral experiments. Statistical comparisons between two groups were conducted by unpaired two-tailed *t* tests. Statistical comparisons among multiple groups were conducted by one-way ANOVA tests and post hoc tests for the indicated comparisons (Dunnett's tests for comparison with a single control and Bonferroni's tests for comparison among different groups). Statistical comparisons for serials of data collected at different time points were conducted by two-way ANOVA tests. The similarity of variances between groups to be compared was tested when performing statistics in SPSS, GraphPad Prism, and Microsoft Excel. The normality of the datasets was assumed for ANOVA and *t* tests and was tested by Shapiro–Wilk tests. When the data were significantly different from the normal distribution, nonparametric tests were used for statistical analysis.

Data Availability. The raw data could be downloaded from https://share.weiyun.com/Cu7qe4IV. All the analyzed data are included in the article and/or *SI Appendix*.

ACKNOWLEDGMENTS. We thank Dr. Isamael Al-Ramahi for the help with *Drosophila* experiments and Dr. Rui Liu for help with analysis of the ITC data. This study was supported by the National Natural Science Foundation of China (grants 81925012, 92049301, and 82050008), the Science and Technology Commission of Shanghai Municipality (Grant 20JC1410900), the Newton Advanced Fellowship (NAF\R1\191045), the Shanghai Municipal Science and Technology Major Project (Grant No. 2018SHZDZX01) and ZJLab, the China National Postdoctoral Program for Innovative Talents (BX20180072), the China Postdoctoral Science Foundation (2018M641916).

1. S. J. Tabrizi, R. Ghosh, B. R. Leavitt, Huntingtin lowering strategies for disease modification in Huntington's disease. *Neuron* **102**, 899 (2019).
2. F. Saudou, S. Humbert, The biology of Huntingtin. *Neuron* **89**, 910–926 (2016).
3. N. S. Trookman, R. L. Rizer, Randomized controlled trial of desonlde hydrogel 0.05% versus desonide ointment 0.05% in the treatment of mild-to-moderate atopic dermatitis. *J. Clin. Aesthet. Dermatol.* **4**, 34–38 (2011).
4. N. Kahanek, C. Gelbard, A. Hebert, Desonide: A review of formulations, efficacy and safety. *Expert Opin. Investig. Drugs* **17**, 1097–1104 (2008).
5. C. Zhu *et al.*, Developing an efficient and general strategy for immobilization of small molecules onto microarrays using isocyanate chemistry. *Sensors (Basel)* **16**, E378 (2016).
6. F. Trettel *et al.*, Dominant phenotypes produced by the HD mutation in STHdh(Q111) striatal cells. *Hum. Mol. Genet.* **9**, 2799–2809 (2000).
7. J. P. Miller *et al.*, A genome-scale RNA-interference screen identifies RRAS signaling as a pathologic feature of Huntington's disease. *PLoS Genet.* **8**, e1003042 (2012).
8. Y. Yao *et al.*, A striatal-enriched intronic GPCR modulates huntingtin levels and toxicity. *eLife* **4**, e05449 (2015).
9. J. P. Miller *et al.*, Matrix metalloproteinases are modifiers of huntingtin proteolysis and toxicity in Huntington's disease. *Neuron* **67**, 199–212 (2010).
10. N. Guo, Z. Peng, MG132, a proteasome inhibitor, induces apoptosis in tumor cells. *Asia Pac. J. Clin. Oncol.* **9**, 6–11 (2013).
11. A. Fribley, K. Zhang, R. J. Kaufman, Regulation of apoptosis by the unfolded protein response. *Methods Mol. Biol.* **559**, 191–204 (2009).
12. Z. Li *et al.*, Allele-selective lowering of mutant HTT protein by HTT-LC3 linker compounds. *Nature* **575**, 203–209 (2019).
13. L. B. Menalled, J. D. Sison, I. Dragatsis, S. Zeitlin, M. F. Chesselet, Time course of early motor and neuropathological anomalies in a knock-in mouse model of Huntington's disease with 140 CAG repeats. *J. Comp. Neurol.* **465**, 11–26 (2003).
14. K. K. Jain, An assessment of iloperidone for the treatment of schizophrenia. *Expert Opin. Investig. Drugs* **9**, 2935–2943 (2000).
15. C. J. Wienken, P. Baaske, U. Rothbauer, D. Braun, S. Duhr, Protein-binding assays in biological liquids using microscale thermophoresis. *Nat. Commun.* **1**, 100 (2010).
16. S. Yang *et al.*, CRISPR/Cas9-mediated gene editing ameliorates neurotoxicity in mouse model of Huntington's disease. *J. Clin. Invest.* **127**, 2719–2724 (2017).
17. D. Young *et al.*, Mutant huntingtin gene-dose impacts on aggregate deposition, DARPP32 expression and neuroinflammation in HdhQ150 mice. *PLoS One* **8**, e75108 (2013).
18. A. Kreidenweiss, P. G. Kremsner, B. Mordmüller, Comprehensive study of proteasome inhibitors against *Plasmodium falciparum* laboratory strains and field isolates from Gabon. *Malar. J.* **7**, 187 (2008).
19. D. J. Klionsky *et al.*, Guidelines for the use and interpretation of assays for monitoring autophagy (3rd edition). *Autophagy* **12**, 1–222 (2016).
20. B. Baldo *et al.*, TR-FRET-based duplex immunoassay reveals an inverse correlation of soluble and aggregated mutant huntingtin in Huntington's disease. *Chem. Biol.* **19**, 264–275 (2012).
21. Q. S. Padiath, A. K. Srivastava, S. Roy, S. Jain, S. K. Brahmachari, Identification of a novel 45 repeat unstable allele associated with a disease phenotype at the MJD1/SCA3 locus. *Am. J. Med. Genet. B. Neuropsychiatr. Genet.* **133B**, 124–126 (2005).
22. Q. Guo *et al.*, The cryo-electron microscopy structure of huntingtin. *Nature* **555**, 117–120 (2018).
23. N. S. Caron, C. R. Desmond, J. Xia, R. Truant, Polyglutamine domain flexibility mediates the proximity between flanking sequences in huntingtin. *Proc. Natl. Acad. Sci. U.S.A.* **110**, 14610–14615 (2013).
24. M. W. Kim, Y. Chelliah, S. W. Kim, Z. Otwinowski, I. Bezprozvanny, Secondary structure of Huntingtin amino-terminal region. *Structure* **17**, 1205–1212 (2009).
25. A. Chiki *et al.*, Mutant Exon1 Huntingtin aggregation is regulated by T3 phosphorylation-induced structural changes and crosstalk between T3 phosphorylation and acetylation at K6. *Angew. Chem. Int. Ed. Engl.* **56**, 5202–5207 (2017).
26. S. J. Tabrizi *et al.*, Phase 1–2a IONIS-HTTRx Study Site Teams, Targeting Huntingtin expression in patients with Huntington's disease. *N. Engl. J. Med.* **380**, 2307–2316 (2019).
27. S. Tomoshige, S. Nomura, K. Ohgane, Y. Hashimoto, M. Ishikawa, Discovery of small molecules that induce the degradation of Huntingtin. *Angew. Chem. Int. Ed. Engl.* **56**, 11530–11533 (2017).
28. S. Sarkar, D. C. Rubinsztein, Huntington's disease: Degradation of mutant huntingtin by autophagy. *FEBS J.* **275**, 4263–4270 (2008).
29. S. Yu, Y. Liang, J. Palacino, M. Difiglia, B. Lu, Drugging unconventional targets: Insights from Huntington's disease. *Trends Pharmacol. Sci.* **35**, 53–62 (2014).
30. A. Weiss *et al.*, Single-step detection of mutant huntingtin in animal and human tissues: A bioassay for Huntington's disease. *Anal. Biochem.* **395**, 8–15 (2009).
31. J. Ko, S. Ou, P. H. Patterson, New anti-huntingtin monoclonal antibodies: Implications for Huntingtin conformation and its binding proteins. *Brain Res. Bull.* **56**, 319–329 (2001).
32. A. Weiss, A. Roscic, P. Paganetti, Inducible mutant huntingtin expression in HN10 cells reproduces Huntington's disease-like neuronal dysfunction. *Mol. Neurodegener.* **4**, 11 (2009).